Eur. Phys. J. D **16**, 173–176 (2001)

THE EUROPEAN PHYSICAL JOURNAL D

EDP Sciences

Magnetic studies on mass–selected iron particles

R.–P. Methling[a], V. Senz, E.–D. Klinkenberg, Th. Diederich, J. Tiggesbäumker, G. Holzhüter, J. Bansmann, and K.H. Meiwes–Broer

Fachbereich Physik, Universität Rostock, D–18051 Rostock, Germany

Received 1st December 2000

Abstract. We have investigated the magnetic properties of mass–selected iron clusters using the Magneto–Optical Kerr effect (MOKE) in longitudinal geometry. For the production of these clusters, a newly developed continuous arc cluster ion source (ACIS) was applied. The source is based on cathodic arc erosion in inert gas environment and subsequent expansion into high vacuum. Its intensity and stability allows mass selection within a wide size range. The source efficiency is demonstrated in deposition experiments and transmission electron microscopy. For mass–selected iron particles deposited into a silver matrix we could observe a change in the magnetic behaviour from ferromagnetism to superparamagnetism around a size of 10 nm at room temperature.

PACS. 36.40.Cg Electronic and magnetic properties of clusters – 61.46.+w Nanoscale materials: clusters, nanoparticles, nanotubes, and nanocrystals – 78.20.Ls Magnetooptical effects

1 Introduction

Nanoscaled metal particles are known to exhibit physical properties which remarkably deviate from those of the corresponding bulk. The deposition of clusters and their magnetic properties on surfaces attract increasing interest in fundamental and applied research since they are supposed to serve as key elements in potential technological applications [1]. A crucial point in this context turns out to be a stable and intense cluster flux of tunable particle size.

Preparation techniques such as mechanical milling of fine powders or annealing of supersaturated solid solutions provide fairly high rates but only crude control of the cluster size can be achieved. However, it has been shown that the size of the particles is in general a quite sensitive parameter. In contrast, cluster–beam synthesis is characterized by the deposition of preformed material in the nanometer range. Here, metal vapor thermalizes and supersaturates in a cooling environment which leads to cluster aggregation. The nucleation rate and hence the size distribution of the clusters depends on the pressure and the temperature of the seeding gas and the metal vapor pressure. In the case of pulsed cluster sources many groups apply laser evaporation [2] or arc erosion based techniques [3] where the cluster beam is created in a high intensity but with low duty cycles. Continuous methods apply lower gas pressures and are mostly based on thermal evaporation [4], sputtering techniques [5], or hollow cathode sputtering [6].

In order to improve the cluster beam intensities we developed a new continuously working source [Patent application number 10135434.7 at the German Patent and Trade Mark Office]. It provides an intensive cluster beam with a broad size distribution. This allows downstream the combination with a rough mass separation unit yielding intensities sufficient for the deposition of thick layers as well as the application of a static quadrupole deflector yielding a moderate cluster flux of a narrow size range. A cathodic arc with erosion rates of ≈1 mg/s serves as a powerful tool for the production of metal vapor. In order to generate the cluster beam this method is combined with gas aggregation. Arc currents of some ten amps yield milligrams of metal vapor per second involved in the aggregation process. Using a special hollow cathode geometry a significant part of the unconsumed material can be recycled by redeposition on a source electrode. In addition, there is a high amount of charged clusters due to the arc discharge.

Below we demonstrate the operation of this new device (ACIS–arc cluster ion source) and especially its use for the production of nanoscaled magnetic deposits. Magnetic particles in the nanometer size range are known to undergo superparamagnetic relaxation at a certain temperature with spatially fluctuating moments. We study iron clusters produced by the ACIS by means of Magneto–Optical Kerr effect (MOKE) and focus our attention on the interesting size range of about ten nanometers.

2 Experiment

The experimental setup for cluster generation and deposition is shown in Fig. 1. The source electrodes are water–cooled since the power consumption amounts to several

[a] e-mail: rm040@physik.uni-rostock.de

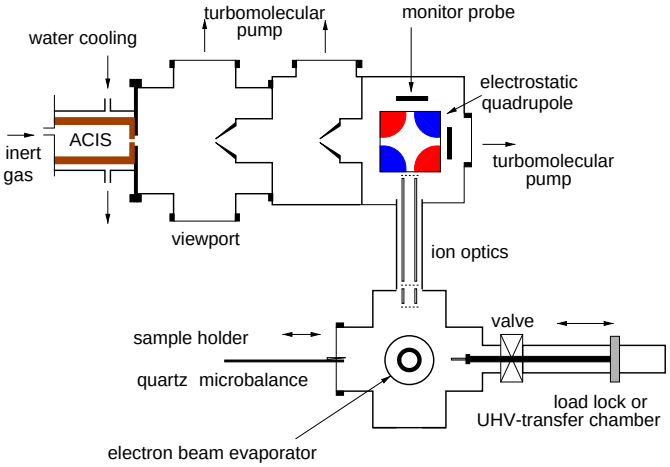

Fig. 1. Experimental setup of the new cluster beam machine containing the ACIS, the mass separation unit and the deposition chamber.

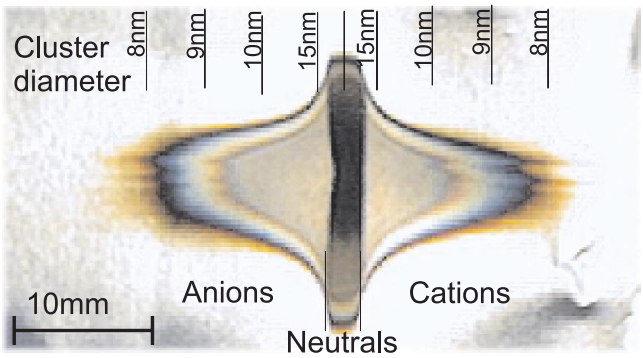

Fig. 2. Iron clusters deposited with a rough mass selection onto an aluminium foil in a distance of 15 cm from the source. The photograph was taken after 5 min of source operation. The central deposit originates from very large and from neutral clusters. The length scale on top of the image displays the correspondingly calculated particle sizes.

hundred watts. Starting at an argon seeding gas pressure of some millibar in the source chamber, the beam passes several differential pumping stages within 0.5 m until it reaches the quadrupole chamber. There, the pressure is about 6 orders of magnitude lower than in the source chamber. From the third pumping stage the beam can be transfered to the UHV deposition chamber.

Since the particle velocity is determined by collisions with the argon seeding gas the kinetic energy directly depends on the number of atoms per cluster N. Thus a rough but efficient mass separation can be obtained by means of passing the (even unskimmed) beam through an electric field. Here the charged clusters with lower energy (the lower N) will experience a stronger deflection whereas the high energetic ones undergo a weaker deflection. This can be realized by applying an electric field to plane electrodes in the first chamber directly behind the source.

In order to achieve mass filtering with higher resolution, the energy and thus mass selecting properties of an electrostatic quadrupole deflector are very useful, see Fig. 1. Positively and negatively charged mass–selected particles are deflected by 90° (in opposite directions) in the electric field. The clusters are guided by an ion optic to the deposition position. A quartz microbalance in the last vacuum chamber serves to monitor the deposition rate. A load–lock system or an ultrahigh vacuum transfer chamber can be mounted on the opposite side of this vacuum chamber. The load–lock system allows a fast entry of a sample from ambient conditions into the vacuum system. A thermal evaporator enables a capping of deposited clusters against oxidation as well as co-evaporation of the clusters into a matrix.

After deposition, the cluster samples are transferred into a transmission electron microscope, or into an UHV–MOKE system. There, hysteresis curves are measured in longitudinal geometry, *i.e.* with the magnetic field in the surface plane and in the plane of light incidence. A magnetic field up to 5 kOe is applied by an external electromagnet. Noise suppression is achieved by modulation of the laser beam intensity and lock–in signal processing.

3 Results and discussion

3.1 Characterization of cluster beam

Generally, the construction of the source allows the use of any solid and conductive material. Up to now titanium, aluminium, copper, and stainless steel as well as iron have been successfully tested. Here, we will report on clusters produced with a pure iron target (99.7%).

By means of deposition and difference weighting, a typical mass flux of some μg per second on a sample of 15 mm diameter is found directly behind the source, this means some hundred nanometers per minute. Using higher source pressures one can see the deposited material through a viewport already within a second.

For a rough estimate of the beam content we separate particles by their size in an electric field placed in the first chamber. The resulting deflection profile can easily be studied by the bare eyes, just by observing the deposit behind the electric field (see Fig. 2). Clearly the beam contains a large fraction of charged clusters. We estimate a total fraction of 50% of the particles being charged. Thus, the great advantage of this source is that an extra ionisation is not necessary. Both anionic and cationic particles are present having approximately the same intensity and mass distribution. Using ion trajectory simulation the cluster size is estimated as is given in the top of the Fig. 2. With the parameters chosen here the cluster deposition rates range around some hundred nanometers per minute. Thus, the source is capable of producing micrometer–thick films of mass–separated iron cluster deposits at least for particle diameters D between five and several tens of nanometers.

In order to determine the deposition rate more quantitatively, roughly size–separated iron clusters ($D = 10 \pm 3$ nm) are deposited on a graphite substrate

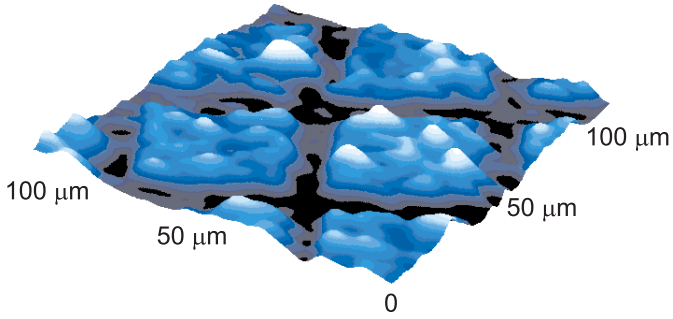

Fig. 3. AFM image of roughly size–separated ($D = 10 \pm 3$ nm) iron clusters deposited on a graphite substrate through a mesh having a periodicity of 70 μm. The maximum height is approximately 4 μm.

and investigated by a atomic force microscopy (AFM). A mesh (with a 70 μm $\times$ 70 μm periodicity) acting as a mask is fixed at the surface and removed after deposition. The structure of the mesh is clearly visible as well as the cluster coating (Fig. 3). From the height difference between the exposed and the shielded areas we deduce a deposition rate of 5 nm/s.

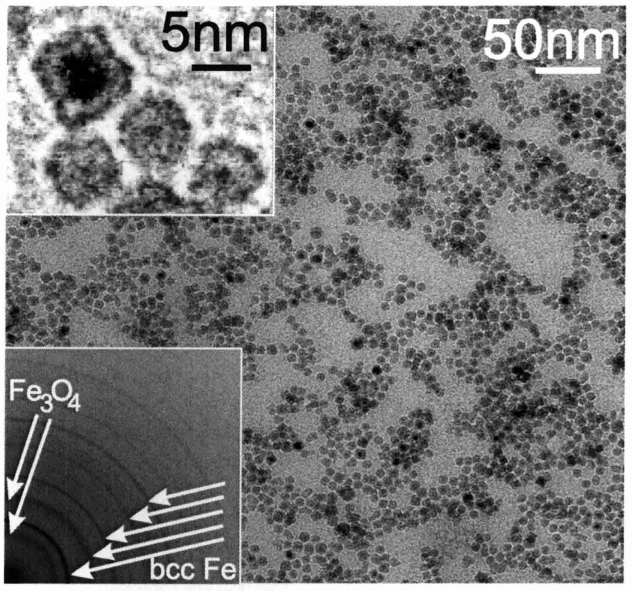

Fig. 4. TEM image of mass–selected iron clusters with a mean diameter of about 5 nm (*cf.* upper inset). Bottom inset: Beside the bcc iron diffraction pattern additional rings resulting from, *e.g.*, Fe_3O_4 are present with lower intensity.

3.2 Transmission electron microscopy

The high cluster ion flux of the ACIS allows enhanced mass filtering which is realized by means of the electrostatic quadrupole deflector with a resolution of $m/\Delta m \approx 12$. The monitor current ranges to about 500 pA ($\sim 10^9$ clusters per second) for cluster sizes between 10^2 and 10^5 atoms.

In order to control the performance of the mass selector, transmission electron microscopy (TEM) has been carried out. For this purpose the voltage of the quadrupole deflector is set to a particle size of 7,300 $\pm$ 600 atoms. Figure 4 shows the result for mass–selected iron clusters deposited onto a commercial electron microscopy grid. Before deposition the grid was covered by an amorphous carbon film that supports the clusters. The particles are well–separated having a mean diameter of $D = 5$ nm in good agreement with the calculated cluster size of (5.4$\pm$0.2) nm. Furthermore, the image indicates that the clusters can diffuse on the surface that, at higher coverages, leads to a percolation of the deposited clusters. Electron diffraction reveals that these particles consist of bcc iron crystallites. Additional traces of Fe_3O_4 can be most probably attributed to partial oxidation of the outer shells. The latter results obviously from the transport to the microscope under ambient conditions.

3.3 Magnetic properties studied by MOKE

Magnetization curves were recorded by means of Magneto–Optical Kerr effect. Here, the rotation of the polarization plane of, *e.g.*, *s*–polarized incident light causes a *p*–polarized component as a direct measure of the sample magnetization. Magneto–optical techniques have been widely applied in surface magnetic research [7] and recently also on cobalt cluster magnetization measurements [8].

The transition from superparamagnetic to ferromagnetic state occurs at a certain temperature–dependent volume. At this so-called blocking volume the energy necessary for changing the magnetization direction KV (with K being the anisotropy constant and V the particle volume) approaches the thermal energy k_BT. Thus, the magnetization of a mono-domain particle may fluctuate over the anisotropy energy barrier leading to vanishing remanence and coercivity. In the case of spherical iron particles this volume corresponds to a diameter of about 11 nm at room temperature [9].

In order to follow this transition we prepared samples with (24,000 $\pm$ 2,000) and (73,000 $\pm$ 6,000) atoms per cluster embedded in a silver matrix on a Si(111) substrate. Supposing spherical shape and iron bulk lattice constant, this corresponds to $D = (8.1 \pm 0.2)$ nm and (11.7 ± 0.3) nm, respectively. Fig. 5 shows the measured normalized magnetization M/M_S *versus* the applied field H. Whereas both samples exhibit very similar sigmoidal–shaped magnetization curves, the sample with bigger clusters is characterized by a slightly opened hysteresis loop. The extracted normalized remanence $M_R\,/\,M_S$ amounts to $(23 \pm 2)\%$ and the coercivity to (0.10 ± 0.01) kOe. Since the magnetization is not completely saturated the value of the remanence is probably overestimated by a few percent. For the second sample with smaller clusters the remanence vanishes indicating the completed transition to the superparamagnetic phase. In order to confirm this statement,

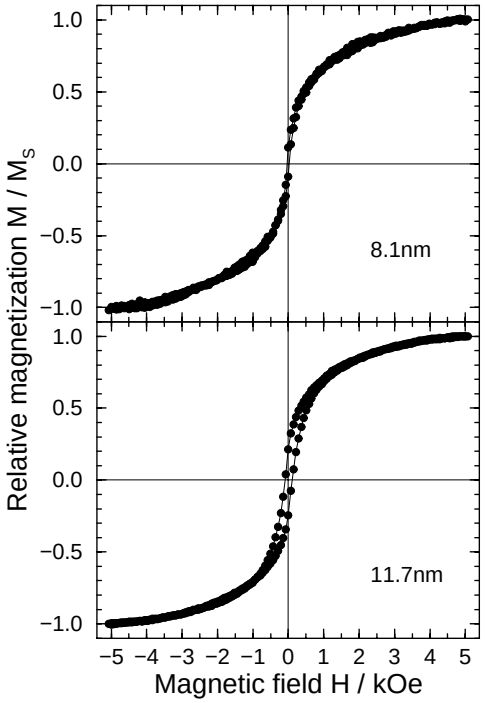

Fig. 5. Room–temperature hysteresis curves of mass–selected iron clusters with diameters of 8.1 nm and 11.7 nm, respectively, in silver matrix, as measured by Magneto-Optical Kerr effect.

more detailed, temperature–dependent measurements are in preparation.

4 Conclusion

An intense arc-based continuous cluster source (ACIS) has been developed. Its efficiency allows the production of mass–selected metal particles with high flux. The broad mass distribution opens the possibility of the particle size over a wide range. Magnetization measurements on cluster deposits from the ACIS using Magneto–Optical Kerr effect carried out at room temperature reveal the transition from the ferromagnetic to the superparamagnetic phase at a particle diameter of about 10 nm.

Financial support by the European Community within the Brite–Euram Project BE 97-4264 and the Deutsche Forschungsgemeinschaft (SFB 198) is gratefully acknowledged.

References

1. *Metal Clusters at Surfaces: Structure, Quantum Properties, Physical Chemistry*, edited by K.H. Meiwes–Broer (Springer, Heidelberg, 2000).
2. U. Heiz, F. Vanolli, L. Trento, W.-D. Schneider, Rev. Sci. Instr. **68**, 1986 (1997).
3. G. Ganteför, H.R. Siekmann, H.O. Lutz, K.H. Meiwes–Broer, Chem. Phys. Lett. **165**, 293 (1990).
4. F. Frank, W. Schulze, B. Tesche, J. Urban, B. Winter, Surf. Sci. **156**, 90 (1985).
5. H. Haberland, M. Mall, M. Moseler, You Qiang, T. Reiners, Y. Thurner, J. Vac. Sci. Technol. A **12**, 2925 (1994); K. Bromann, C. Félix, H. Brune, W. Harbich, R. Monot, J. Buttet, K. Kern, Science, **274**, 956 (1996).
6. A.C. Xenoulis, P. Trouposkiadis, C. Potiriadis, C. Papastaikoudis, A.A. Katsanos, A. Clouvas, Nanostruc. Mat. **7**, 473 (1996).
7. Z.Q. Qiu, S.D. Bader, Rev. Sci. Instr. **71**, 1243 (2000).
8. S. Padovani, I. Chado, F. Scheurer, J.P. Bucher, Phys. Rev. B **59**, 11887 (1999).
9. C.P. Bean, J.D. Livingston, J. Appl. Phys. **30**, 120S (1959).